# EXPERIMENTAL PROBES OF THE OPTICAL PROPERTIES OF PHOTONIC CRYSTALS

Willem L. Vos*, Henry M. van Driel†, Mischa Megens‡, A.Femius Koenderink, and Arnout Imhof§

*van der Waals-Zeeman Instituut, Universiteit van Amsterdam, Valckenierstraat 65, 1018 XE Amsterdam, The Netherlands*

## 1 INTRODUCTION

The propagation of electromagnetic radiation in three-dimensional periodic dielectric structures is strongly modified if the wavelength of the radiation is on the order of the lattice spacing.[1–5] Such structures are called photonic crystals. Their periodicity gives rise to photonic band structures in a way that is analogous to electronic band structures.[6] Much of the recent interest in photonic crystals stems from the possibility of making lattices for which there exists a range of frequencies in which waves cannot propagate in any direction in the crystal.[1–4] Such a photonic band gap occurs if the coupling between light and lattice is sufficiently strong. The coupling is conveniently gauged by the polarizability per volume of the scatters.[7] If a lattice could be constructed with a photonic band gap at optical frequencies, this would result in spectacular effects such as the inhibition of spontaneous emission,[3] and localization of light.[4]

Following the first demonstration of a photonic band gap in the microwave range by Yablonovitch *et al.*,[8] there have been many attempts to fabricate crystal that will work at optical frequencies. This requires a structure that has a lengthscale that is about a ten thousandth of the size of the microwave crystals. In 1996, teams from Siemens[9] and the University of Glasgow[10] made crystals with two-dimensional bandgaps, that is, bandgaps for light confined to a plane. Grüning *et al.*[9] electrochemically etched silicon to produce a gap at a wavelength $\lambda \sim 5\mu$m, while Krauss *et al.*[10] performed lithography on AlGaAs to obtain a gap near $\lambda = 850$ nm. In the past two years, Lin *et al.*[11] and Noda *et al.*[12] took the next logical step: using advanced techniques, several microstructured semiconductor layers were stacked to make three-dimensional crystals. They created structures with stop gaps at telecom wavelengths in the near-infrared.

Stacking, however, is not the only way to make three-dimensional crystals. An easier method is to make photonic crystal from self-organizing systems such as colloidal suspen-

*Author for correspondence: wvos@wins.uva.nl

†Permanent address: Department of Physics, University of Toronto, Toronto, Canada, M5S 1A7

‡Present address: Department of Physics, Princeton University, Princeton NJ 08544, U.S.A.

§Present address: Debye Instituut, Universiteit Utrecht, Princetonplein 1, 3584 CC Utrecht, The Netherlands

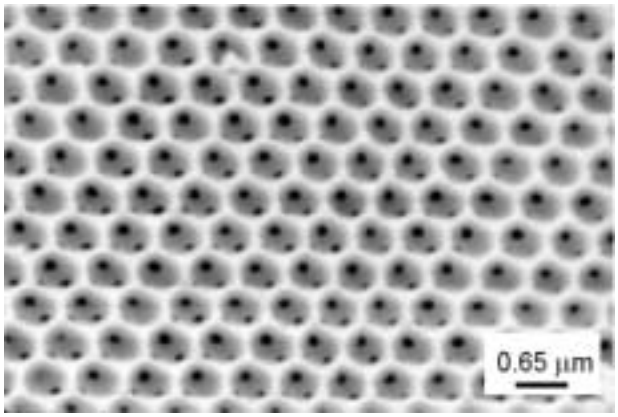


*Figure 1:* Scanning electron micrograph of the surface of an air-sphere crystal in titania with $a = 913 \pm 9$ nm. The scale bar is 0.65 $\mu$m long. The hexagonal arrangement of voids in this near-perfect section are an *fcc* (111) plane. From Ref. 30.

sions. These systems have naturally the right structure size for the optical range, but unfortunately only a small refractive index variation, hence a weak coupling. Recently, however, self-organizing systems have been used as templates to structured materials with high refractive (see, e.g., Ref. 13, 14). This has lead to the development of extended three-dimensional photonic crystals[15–17] that strongly interact with light.[18] The conceptual ease of making such so-called air-sphere crystals has sparked an explosion of activities in the field (see, e.g., Ref. 14, 19).

From early on, the theory of photonic crystals has been well developed.[1, 2, 20, 21] To keep theory for three dimensions tractable, infinitely large perfect crystals are usually described. In practice, however, the physics is certainly affected by the finite size of the crystal or by inevitable disorder.[6] In this contribution, we review experiments that probe the optical properties of photonic crystals; we aim to compare experimentally measurable quantities to theoretical models.

## 2 EXPERIMENTAL

Our experiments are mainly concerned with systems made by self-organization. We use colloidal suspensions of particles with high size monodispersities and sharp interfaces.[22, 23] Photonic crystals made from colloids are carefully grown, with a wide range of particle volume fractions ($\phi$),[7, 23–26] and artificial opals were made by slowly drying the crystals.[7, 16] Colloidal particles with intentionally low dye content (see Ref. 27) were made to grow photonic crystals with internal light sources.[25, 26, 28, 29] Strongly interacting crystals of air spheres in titania were developed[16](cf. Fig. 1), and carefully characterized. It appears that the air-sphere crystals possess a titania backbone with a dielectric constant of 6.3-6.5 in the IR-visible region.[30] Recently, electrochemistry has been applied as a new means to make crystals with unexpected optical properties.[31] The samples are extensively characterized by a range of techniques, such as optical microscopy and reflectivity, scanning electron microscopy, Raman scattering, x-ray diffraction. In particular, we have found that small angle x-ray scattering using synchrotron radiation (at the ESRF) is a highly valuable tool to study photonic crystals non destructively in great detail and document highly ordered crystals.[22–24, 30, 32]

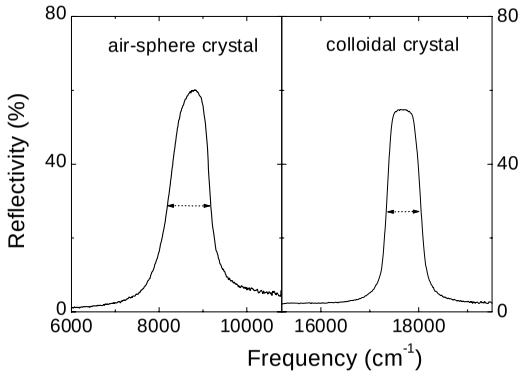


*Figure 2:* Reflectivity measured at normal incidence for an air-sphere crystal in $TiO_2$ with $a = 860$ nm (left, solid curve) and for a colloidal crystal of $R = 101$ nm polystyrene spheres in methanol with $a = 338$ nm (right, dashed curve) as a function of frequency ($\omega/2\pi c$) in wave numbers. The full widths at half maximum are indicated by the horizontal arrows.

## 3 BRAGG DIFFRACTION AND STOP GAPS

The interaction between radiation and photonic crystals causes the splitting of degenerate bands for wave vectors on the surface of the Brillouin zone, and the appearance of frequency gaps. Waves with frequencies within these stop gaps are Bragg diffracted and cannot propagate. Stop gaps are associated with every propagation direction with respect to a set of lattice planes. The widths of stop gaps increase with the interaction strength between light and the crystal. Since stop gaps are the precursors to a photonic band gap, the study of their optical properties is essential. Here, we will discuss several techniques to study stop gaps, notably their widths, since the center frequencies, that are determined by the lattice spacing and the average refractive index, are well understood.[7, 33] The mechanism how a photonic band gap actually develops, namely from multiple Bragg diffraction, is treated in section 7.

### 3.1 Reflectivity

Reflectivity is perhaps the oldest way to study Bragg diffraction of crystals.[5, 6] In essence, light with frequencies inside a stop gap is diffracted and rejected from the crystal. Figure 2 shows the reflectivity as a function of frequency for a crystal of air spheres in titania, and for a colloidal crystal of polystyrene spheres in methanol. The air-sphere crystal, with lattice parameter a = 860 nm, shows a strong Bragg peak at 8800 $cm^{-1}$, with a large relative width (full width at half maximum (FWHM) divided by the center frequency) of 11.3 %, and a maximum reflectivity of 60 %. The colloidal crystal shows a Bragg peak at 17600 $cm^{-1}$, with a relative width of 4.0 %, and a maximum reflectivity of 55 % on a flattish top. The larger width of the Bragg peak of the air-sphere crystal is due to the larger spatial variation of the refractive index, which results in stronger coupling. Several features of the experimental curves are remarkable compared to the ideal peak shape predicted by dynamical diffraction theory:[5] the experimental peaks are rounded and have maxima less than 100 %. An ideal diffraction peak has a flat top with 100 % reflectivity, that abruptly falls off at the edges. The width of the top is equal to the width of the stop gap and the FWHM is only a few percent larger. In presence of absorption, diffraction peaks become rounded and asymmetric with maxima less than 100 %, but the FWHM remains the same. We can exclude absorption as the cause for the experimental features, but extinction — that also removes energy from incident or diffracted beams — likely plays a role. Extinction may be due to various imperfections, e.g.,

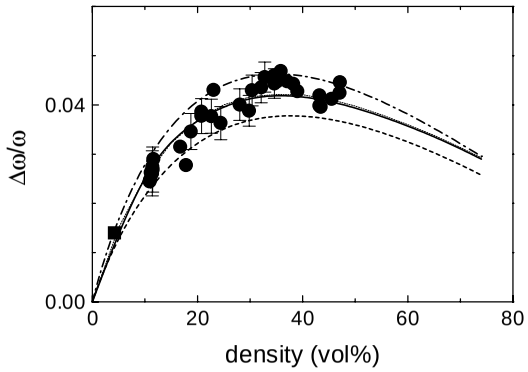


*Figure 3:* Relative width of Bragg peaks for crystals of polystyrene colloids, with various radii, in water or methanol as a function of the particle density, measured at normal incidence. We define $\Delta\omega$ as the full width at half maximum, and $\omega$ as the center frequency.[34] The curves are theoretical calculations using the dynamical diffraction theory (dotted curve), band structure calculations and KKR theory (both solid curve), and the E-field expansion with two bands (dashed-dotted curve).

mosaic spread that causes light to be diffracted non-specularly, grain boundaries between simultaneously illuminated crystal domains that scatter light diffusively, or non-crystalline features that sometimes occur on the surfaces of air-sphere crystals (cf. Fig. 2 of Ref. 16). At this point, we caution that for zero photonic interaction a diffraction peak may broaden due to crystal faults such as strain or finite crystal domains ("Scherrer broadening").[5] Thus, the degree of crystalline order should be checked independently from experiments that probe photonic crystal properties. Therefore, we have done extensive characterization.

From the consideration of theoretical diffraction peaks above, we propose that the FWHM of a diffraction peak is a robust measure of the width of a stop gap. In Fig. 3, we plot the relative widths for crystals of polystyrene colloids, with various radii, in water or methanol as a function of the particle density (for a preliminary account, see Ref. 34). The data were measured on many different samples that were prepared with various amounts of deionization. For each sample, we measured reflectivity as a function of height in the capillary; hence, as a function of particle density, since colloids sediment under gravity. Figure 3 shows that with increasing particle density, the relative width increases, levels off near 40 vol$\%$, and then decreases. In earlier transmission experiments,[35] the widths were difficult to resolve and consequently suffered from a relatively large uncertainty. For comparison, we have calculated the relative widths with several theories shown in Fig. 3: *(i)* plane-wave band structure calculations,[2, 20] *(ii)* plane-wave band structures in the two band approximation,[36] *(iii)* dynamical diffraction theory,[5, 37] and *(iv)* KKR multiple scattering theory.[38] The experimental widths agree very well with all calculations, confirming the hypothesis that the FWHM of a diffraction peak is a good measure of the width of a stop gap. Similarly, relative peak widths of air-sphere crystals match with stop gap widths calculated for a model of close-packed air spheres in a completely infiltrated backbone[18] (with too large a filling fraction) and match very well with an appropriately optimized model.[39, 40]

Using the dynamical diffraction theory, one can derive that the relative width of a stop gap is proportional to the polarizability $\alpha$ per volume $v$,[37] that is a very useful gauge for a photonic interaction parameter $\Psi$.[7] For (111) diffraction, the proportionality constant is equal to one, within a few percent. We conclude that it is possible to experimentally measure the interaction strength between light and photonic crystals by the relative width of a stop gaps (for fcc crystals usually the L-gap). For crystals of dielectric spheres, one can rewrite the photonic parameter as: $\Psi = 4\pi\alpha/v = 3\phi(m^2-1)/(m^2+2)g(Kr)$, where $m$ is the ratio of the

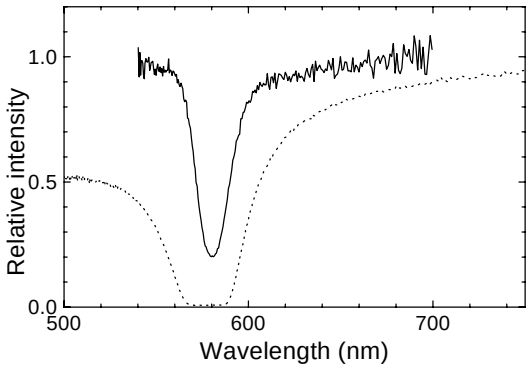


*Figure 4:* Transfer function for light sources inside a crystal (solid curve, relative fluorescence intensity of dye) and transmission for plane waves emitted by a light source far away outside the crystal (dotted curve). Both spectra were taken normal to the *fcc* (111) crystal planes at the same spatial spot, see Ref. 28.

refractive indices of the spheres and the surrounding medium, and $g(Kr)$ is the form factor of the scatterers (here Rayleigh-Gans) as a function of sphere radius $r$ and diffraction vector $K$. This reformulation allows a physical interpretation of Fig. 3: the stop gap first increases because the density of scatterers increases, but then it saturates and decreases because the particles scatter less efficiently (the form factor decreases). Apparently the polarizability of a single unit cell elegantly gauges the interaction between light and a photonic crystal.

### 3.2 Transmission

Transmission of plane waves incident from outside is a well-known method to study photonic gaps.[8] Examples of transmission at normal incidence ($\alpha = 0°$) to (111) lattice planes are shown in Figs. 4 and 5a for colloidal crystals of silica spheres in water[28] and polystyrene spheres in water.[41] The transmission is high at low frequencies (or long wavelengths) and at high frequencies (or short wavelengths) and decreases dramatically towards the edge of the stopgap, thereby forming a deep characteristic "notch." Idealized transmission curves through Bragg planes are expected to be equal to one minus the reflectivity (see above).[5] Hence, the transmission is expected to show a sharply bounded notch, and indeed the stop gap in Fig. 4 (linear transmission scale) decreases to zero with rather abrupt edges. It is expected that the width of the notch at zero transmission is equal to the width of the stop gap. The experimental notch, however, is about 25 nm wide, much wider than values of 11.1–11.7 nm predicted by dynamical diffraction[5, 37] or band structure theories.[20] We have observed this discrepancy in many other cases. A likely explanation for the wide transmission notches is that light samples the complete thickness of the sample, that is, more than a thousand lattice planes, including planes far from the capillary wall that may be less well aligned. In contrast, reflectivity (and emission spectra, see below) probes relatively few crystal planes that are well aligned close to the cell wall and reflectivity from misaligned planes is not detected. These observations are corroborated by results on thin crystals (up to 50 layers) whose transmission agrees well with theoretical estimates that include a significant Scherrer broadening.[42]

It is remarkable that in Figs. 4 and 5a the transmission at frequencies above the stop gap is lower than below the stop gap. This contrasts to idealized transmission curves, that have equal transmission values at low and high frequencies.[5] In experiments by many other workers, a similarly decreasing transmission with increasing frequency is observed, which has been ascribed to a Rayleigh-like scattering from crystal defects by Vlasov *et al.*[43] It is also

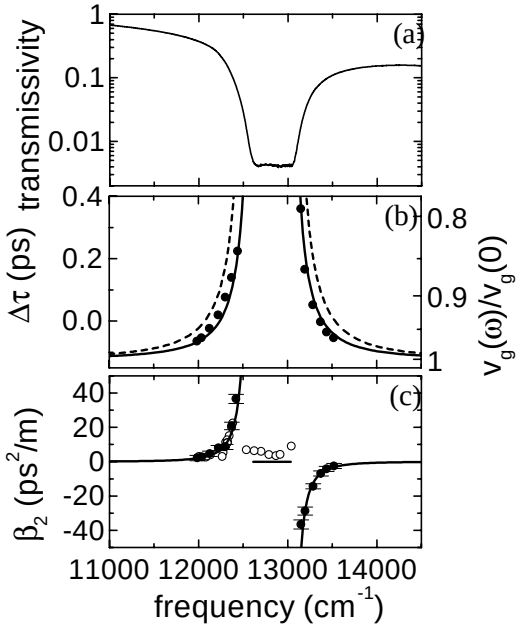


*Figure 5:* (a) Transmission spectrum of a colloidal photonic crystal. (b) Measured pulse delay times ($\Delta\tau$, solid circles) near the L-gap versus the central frequency of the incoming pulses. (c) Group velocity dispersion parameter ($\beta_2$), measured in transmission (solid circles) and reflection (open circles). The solid curves in (b) and (c) represent the dynamical diffraction theory,[5] and the dashed curve in (b) the two-band model for the E-field.[36] From Ref. 41.

interesting that the attenuation in the middle of a stop gap that is apparent on a semilogarithmic scale as in Fig. 5(a), is much lower than theoretically expected on the basis of the number of crystal layers (see also Ref. 37). For comparison, in thin crystals studied with microwaves, with length scales for which precise machining is feasible, the attenuation in the middle of stop gaps agrees well with theoretical estimates, and the transmission below and above stop gaps are in close agreement.[44] These results taken together suggest that attenuation in a stop gap is limited by crystal imperfections (except finite crystal size).

### 3.3 Group Velocity

While continuous wave reflectivity and transmission are very useful to determine the presence of stop gaps, they do not provide full information on the light propagation through the crystal. Time-resolved experiments are essential to reveal the dynamics of the electromagnetic fields in the photonic crystal. In one-dimensional multilayer systems, pulsed-laser experiments have demonstrated extremely short tunneling times at in-gap frequencies,[45, 46] as well as very low group velocities at near-gap frequencies.[47] Pulse slowing was also studied in a synthetic opal.[48] We have used phase-sensitive ultrashort-pulse interferometry[49] to probe the modification of light propagation close to the band edges of a photonic crystal. This technique measures the interferometric cross correlation function of a laser pulse transmitted by the sample with the incoming pulse. In Fig. 5(b) the time delays are plotted versus the central frequency of the incoming pulse. The pulse delay time $\Delta\tau$ is the time delay introduced by the crystal plus the capillary minus an equal distance of glycerol, and can therefore be negative. For comparison, the sample transmission spectrum, measured in a spectrometer with a white light source, is shown in Fig. 5(a). The data clearly demonstrate a large decrease of the group velocity near the edges of the stop gap. The largest time delay measured corresponds to a

pulse propagation speed of only about 80 $\%$ of that far from the gap. This means that the pulse experiences an increased effective path length due to multiple reflections in the crystal.

To describe the data in Fig. 5(b), we used the dynamical diffraction theory,[5] that approximates the displacement field in the crystal by the two strongest Fourier components: the incident and the diffracted waves. The theory yields a dispersion relation $\omega(k)$ that can be differentiated to obtain the group velocity. The input parameters are the refractive indices of water (1.33) and polystyrene (1.59), as well as the particle diameter (222 nm) and the lattice spacing. The (111) lattice spacing is fixed independently by requiring that the predicted location of the stop gap coincides with the center of the transmission minimum, yielding a value of 284 nm. With all parameters fixed, the time delay was calculated for a 0.4 mm crystal and an offset was added to allow for the capillary and index-matching glycerol. The result is shown in Fig. 5(b). The dynamical diffraction theory is seen to describe the data very well. It gives an average refractive index of 1.372 and a relative gap width of 0.032. As an independent check we measured the wavelength-dependent diffraction angle corrected for Snell's law. At $\lambda = 633$ nm the crystal was observed to have a diffraction angle of $54.2^\circ$ degrees, from which we derive a lattice spacing of 286 nm and an average refractive index of 1.366, agreeing with the values above. It has been predicted[21] that the D-field expansion is reasonably accurate for crystals of dielectric spheres but fails badly for dielectric spheres, and the opposite holds for the E-field. Indeed, an analogous theory that keeps the two strongest components of the *electric* field[36] did not describe the data well. We note that the data of Ref. 48 do not distinguish between the expansions. Our result also agrees with a closer inspection of Fig. 3, revealing that the two band E-field model predicts the largest widths. Since measured widths are in principle upper bounds for the "photonic" width, due to possible defect-broadening, this model overestimates the stop gap widths. The dynamical diffraction theory agrees better with the experimental data.

Even though the measurements in Fig. 5(b) explore only one set of lattice planes, one-dimensional models do not describe the data as well as the 3D dynamical diffraction theory. The best mapping of the real 3D crystal onto a 1D multilayer stack was obtained with the model of Lidorikis *et al.*,[50] which also needs no adjustable parameters. This model gives a reasonable correspondence to the data, but the gap width is off by 40 $\%$, resulting in differences with the measured delay times.

### 3.4 Group Velocity Dispersion

We have been able to measure the group velocity dispersion (gvd), since our interferometric technique yields phase information about pulses sent through a sample.[51] The gvd quantifies the relative phase shift of frequencies in a wave packet. The gvd can be interpreted as being inversely proportional to an effective photon mass, in analogy to electronic band structures. This property has not been measured before in photonic crystals. Pulse reshaping, that is present in dispersive systems such as photonic crystals, does not affect the gvd at all whereas it hampers an unambiguous estimation of the group velocity. The measured gvd parameter $\beta_2 = (d^2k/d\omega^2)|_{\omega_0}$, with $\omega_0$ the center frequency of the pulse, is plotted in Fig. 5(c). If the pulse frequency comes to within a few percent of the band edges, the gvd diverges. The measured values are two to three orders of magnitude larger than well-known values for ordinary glass. At the high-frequency side of the stop gap, we find a branch of anomalous dispersion. The cubic coefficient (not shown) was found to be positive on both sides of the gap. The curve in Fig. 5(c) is $\beta_2$ calculated from the dynamical diffraction theory by taking the second derivative of $k$ with respect to $\omega$, using the same parameter values as before. Again, the data are described remarkably well by this theory. In analogy to electrons in semiconductors,[6] our measurements can be interpreted as large effects on the effective photon mass, which is negative below and positive above a gap.

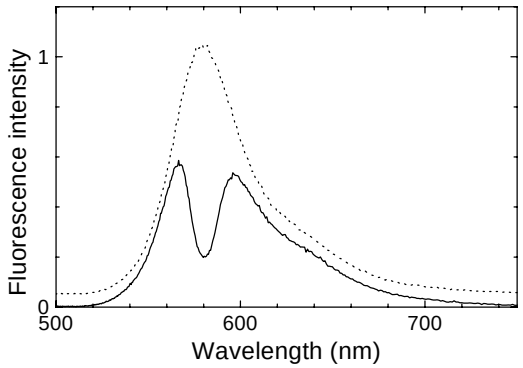


*Figure 6:* Fluorescence spectrum of dye in a photonic colloidal crystal (solid curve) and in a colloidal liquid of spheres (dotted curve, offset by 0.05). Bragg reflection causes a stop gap in the spectrum of the crystal.[28]

By doing the interferometry experiments in reflection, we have succeeded in studying frequencies inside the stop gap. Figure 5(c) shows the resulting data for the gvd. The data agree well with the data measured in transmission outside the stop gap. A dramatic change takes place in crossing the edge of the stop gap: inside the gap, the dispersion is very low and constant. An important conclusion from these experiments is that the gvd naturally distinguishes the edges from the inside of stop gaps. No further interpretation is necessary, in contrast to all other probes of stop gaps.

## 4 EMISSION BY LIGHT SOURCES INSIDE PHOTONIC CRYSTALS

In the previous section, we have seen that the periodic structure of a photonic crystal gives rise to Bragg diffraction, that is associated with stop gaps for propagation in certain directions. In the direction of a stop gap light is excluded from the material. The situation is reminiscent of atoms or molecules in one-dimensional Fabry-Perot cavities.[52, 53, 55] A Fabry-Perot cavity can modify the spontaneous emission rate of atoms or molecules inside.[52, 55] The main difference between Fabry-Perot cavities and photonic crystals is that photonic crystals act as three-dimensional cavities, thereby promising complete control over emission. We investigate the modification of the emission spectrum of light sources inside photonic crystals, and we study their dynamics. Emission spectra of internal sources have been measured before, and stop gaps in these spectra have been observed. Unexpectedly, these stop gaps differ in several respects from those encountered in conventional transmission spectra, e.g., the attenuation and the width of gaps in emission spectra are smaller than in transmission spectra. In time-resolved emission studies, there have been surprising reports of modified lifetimes, up to a factor of 2, even for weakly photonic crystals. We argue that such large changes are not of photonic origin and present a simple model that relates the luminescence lifetimes to the interaction between light and the crystals.

### 4.1 Emission Spectra

We have obtained fluorescence spectra of dye in many different photonic crystals composed of dyed silica spheres in water. A typical example is shown in Fig. 6 and compared to the spectrum of a dilute colloidal liquid of dyed spheres. The crystal changes the fluorescence spectrum of the dye considerably: the spectrum acquires a pronounced stop gap. The

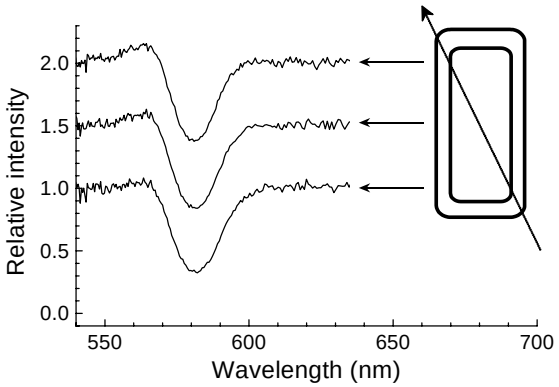


*Figure 7:* Internal transmission spectra (relative fluorescence intensities) for various distances from light source to sample surface. The depth of the light source varies with the depth of the light beam which excites the fluorescence (see schematic drawing). The upper curves have been offset by 0.5 and 1.0 respectively. Each curve corresponds to the position in the sample as indicated.[28]

stop gap is caused by the (111) crystal planes. The crystal planes act as Bragg mirrors for the fluorescence, preventing part of the light to leave the crystal. We observed that the central wavelength of the stop gap depends on the density of spheres in the crystal. We can vary the density and hence tune the stop gap wavelength. As an example, we have carefully tuned the stop gap on the dye emission spectrum in Fig. 6.

We have also measured the transfer functions for various emission directions.[28] Stop gaps are observed for all emission directions. Away from the normal, the central wavelength of the stop gap goes to shorter wavelengths, qualitatively resembling Bragg reflection. The shift of the central wavelength is very well explained using Bragg's law $2d \sin\theta = \lambda/n_{\rm eff}$ with an effective refractive index $n_{\rm eff}$, if allowance is made for refraction at the sample interface using Snell's law. This agrees with earlier diffraction experiments.[7] We note that Bragg's law with an effective Maxwell-Garnett refractive index yields results which closely correspond with dynamical diffraction theory.[5] Emission wavelengths that are equal to the Bragg wavelength at normal incidence, can still propagate in oblique directions. For shorter emission wavelengths, the light is Bragg reflected at a certain angle, but can propagate in other directions, such as the normal one. The resulting variations in fluorescence intensity are familiar from X-ray fluorescence, where they are referred to as Kossel lines.[5]

In Fig. 4, the stop gap in the transfer function is about 20 nm wide. A width between 11.1 and 11.7 nm is predicted theoretically.[20, 5] The width of the stop gap in transmission, however, is much larger. Apparently the course of plane waves through the sample is qualitatively different from that of light generated inside.

It is striking that for the same crystal, the transfer function shows much less attenuation than the transmission of external sources, where the attenuation at the center of a stop gap is appreciable, see Figs. 4 and 6. To elucidate the origin of this difference, we have varied the position of the light source inside the sample as follows (*cf.* inset of Fig. 7); the light which excites the dye is sent at a glancing angle of 30° through the sample. Thus, the beam is close to the front surface at one edge and close to the back surface at the other edge of the sample. By imaging a specific part of the sample on the detector, we select the depth of the emitting sources. The beam waist at the sample measures only 20 $\mu$m FWHM, and the width of the imaged area is 50 $\mu$m, both much less than the 300 $\mu$m sample thickness. The resulting transfer functions are shown in Fig. 7. The outermost curves correspond to regions which are 400 $\mu$m apart on the sample. Surprisingly, the attenuation of the fluorescence stop gap does not depend on the depth of the sources. We checked that the fluorescence originates

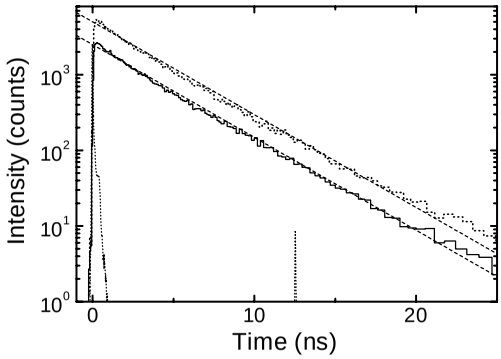


*Figure 8:* Time-resolved intensity for dye in a photonic crystal made of dyed silica spheres (radius 121 nm) in water at 65 vol% (solid curve), and for similar dyed colloids in a disordered dilute reference sample (dashed curve, offset by a factor of 2), at $\lambda$ =577 nm.[25, 29] The mean lifetimes of 3.54±0.02 ns are indicated by straight dotted lines. The narrow spike at 0 ns is the instrument response and the weak spike at 12 ns is an afterpulse from the laser.

in the bulk of the sample by photochemically bleaching the dye close to the surface with an intense laser beam tuned to a Bragg reflection. The bleaching did not deepen the stop gap. We can also exclude the possibility that the depth dependence is washed out by a diffuse excitation beam: Fig. 4 shows that there is a large transmission of light at the excitation wavelength (488 nm). Indeed we observed a well-defined blue beam behind the sample. From the observation that the stop gap is already present for sources close to the surface, we conclude that the stop gap takes only few crystal planes to build up. It is remarkable that the attenuation in the stop gap does not increase with further increasing depth of the source. Apparently the attenuation in the stop gap in the transfer function is mostly determined close to the surface but not by the bulk of the crystal.

From the comparison between the transfer function and the transmission spectrum (see Fig. 4), it is clear that a considerable amount of fluorescence light with wavelengths in a stop gap reaches the sample surface and then leaves the crystal in the direction of a stop gap. The explanation for this phenomenon is that defects near the surface of the crystal scatter in all directions, including the direction of the stop gap. The phenomenon can be understood as follows: Light emitted in the direction of a stop gap is attenuated, but the light can propagate perfectly well in other directions (see Ref. 28 and Fig. 12). The light will be scattered by a small concentration of defects that always occur in crystals.[6] Radiation scattered by defects deep inside the crystal will experience a similar attenuation as in a plane wave experiment. If light is scattered by defects close to the surface of the crystal, this radiation will appear unattenuated outside, even in the direction of a stop gap, because the light traverses only a thin layer of photonic crystal. Thus, light appears in the direction of a stop gap. The internal sources emit light in a large solid angle of nearly $2\pi$ to the exit surface, hence an appreciable contribution is expected compared to the light that directly propagates into the $0.016\pi$ solid angle of the detector. In contrast, in a plane wave transmission spectrum the contribution of diffuse scattering is hardly noticeable. The reason is that the beam that propagates to the detector is well collimated, whereas the randomly scattered light is spread over $4\pi$ solid angle. This elucidates why the stop gap in fluorescence is shallower than the deep stop gap in plane wave transmission spectra (*cf.* Fig. 4).

Very recently, we have obtained emission spectra of dye inside air-sphere crystals.[54] The spectra appear to be strongly modified by multiple Bragg diffraction effects, see section 7.

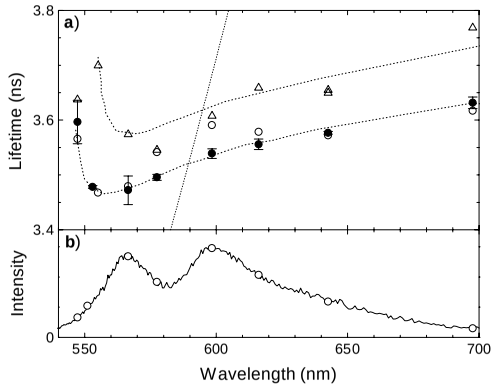


*Figure 9:* (a) Excited state lifetime of dye inside photonic crystals (open and solid circles, densities of 65 and 53 vol%, respectively) and in a colloidal liquid (triangles), at various wavelengths in the dye spectrum. The solid circles are an average of two measurements, indicated by error bars. The dotted curves are guides to the eye.[25] The emission spectrum of the 65 vol% crystal is shown in (b) for comparison. The open circles indicate the wavelengths at which lifetimes were measured.

### 4.2 Time Resolved Emission

We have studied time resolved emission of dye in photonic crystals. Our system consists of dye-doped silica spheres in water, with a dielectric contrast of 1.2. The dye is covalently attached to the silica spheres and covered by a silica layer. The chief advantage of our system is the ability to confidently compare the crystal with a reference system consisting of the same spheres in a random arrangement. Figure 8 shows two typical time-resolved fluorescence traces, one of dye in a colloidal crystal and one of dye in a colloidal liquid, measured at a wavelength of 577 nm, corresponding to the crystal's stop gap. The measured fluorescence intensities extend over three full decades. The fluorescence decay is very close to a single exponential, which indicates that unwanted non-radiative effects are effectively reduced by the low dye concentration and the protective cover layer.[27] From the fluorescence decay curves we have obtained lifetimes by calculating the average time at which a photon is detected. The lifetimes for the curves in Fig. 8 are both 3.5 ns, *i.e.*, there is hardly any difference in lifetime between a crystal and a colloidal liquid.

Figure 9 shows fluorescence lifetimes as a function of wavelength in the dye spectrum, for two photonic crystals with different densities, and for a colloidal liquid. The densities of the crystals that we have used were 65 and 53 vol%. Due to the density difference the center wavelength of the stop gaps of the crystals differ: for the low density crystal the stop gap is at $617 \pm 9$ nm, whereas for the high density crystal it is at $582 \pm 2$ nm. Since the stop gap wavelengths of the two crystals differ, the densities of optical modes of the two crystals should also display different wavelength dependencies. This difference should become visible in the measured lifetimes. However, the measured lifetimes in these crystals do not show a significant wavelength dependence. The variations in lifetime are on the order of only 0.05 ns, or 2 %. This observation shows that the influence of the photonic band structure on lifetime in these crystals is surprisingly small, considering the large changes in the spectra. Below we will resolve this seeming paradox.

We can interpret the variation in lifetimes by comparing this variation to the width of the stop gaps of the crystals. A simple model connects the lifetimes to the width of the stop gaps, and it explains why the photonic crystals under study have only a small influence on lifetimes. In the direction of a stop gap, light cannot be emitted since the zero point fluctuations are expelled from the photonic crystal by repeated reflection from the lattice planes.

Since our weakly photonic crystals do not have a band gap, light at a specific wavelength is reflected only for certain directions, in the other directions the emission persists. We expect that the relative change in radiative lifetime of the fluorescent molecules is of the order of the solid angle subtended by the Bragg reflections, compared to the full $4\pi$ solid angle which is available in the absence of a crystal, see Fig. 16. For atoms in a Fabry-Pérot interferometer the results of this approach are in excellent agreement with the experiments of Heinzen *et al.*[52] It turns out that the relative change in excited state lifetime is in good approximation equal to four times the relative width of the (111) stop gap in the spectrum;[25] the factor of $4$ stems from the four pairs of $\{111\}$ planes. From our stop gap width of $2\,\%$, we estimate a change in radiative lifetime of only $0.3$ ns. The estimated radiative lifetime change provides an upper bound for changes in fluorescence lifetimes. This upper bound is consistent with the measured variations in $\tau$ of the crystals in Fig. 9. Apparently a large change in fluorescence spectrum can coincide with only a minor change in fluorescence lifetime, which resolves the paradox mentioned above.

The observed small change in lifetime contrasts with earlier results. Martorell and Lawandy found a change in lifetime by a factor $1.8$ for their crystals of polystyrene spheres in water with rhodamine dye dissolved in the liquid.[56] It has been suggested that their large change in lifetime is not caused by photonic band structure but by other factors such as chemical interactions and adsorption of the dye on the sphere surfaces. Petrov *et al.*[57] have measured fluorescence of dye in a polymer-filled opal. The decay curves were fitted with a distribution of lifetimes, in which the short lifetimes were about half as long as the long lifetimes. The nonexponential decay was attributed to a modified density of optical modes while chemical or nonradiative effects were not considered. The fluorescence lifetimes were not spectrally resolved to demonstrate the anticipated variation in density of optical modes with wavelength. Surprisingly, lifetime changes were noted for wavelengths at the low frequency side of the stop gap, where the solid angle subtended by the Bragg reflections is least and our simple argument predicts no lifetime change. In both of the previous studies, the widths of the stop gaps of the samples are the same as the width of the stop gaps of our crystals, hence the change of the radiative lifetimes should in both cases be similar to the data in Figs. 8 and 9.

## 5 DISORDER

Disorder in photonic crystals is of fundamental interest in the study of Anderson localization of light, as witnessed by one of the first proposals for the study of photonic crystals.[4] Anderson localization[58] of light is an interference effect in random multiple scattering of light, which is commonly studied in disordered optical materials.[59, 60] Disorder, always present in any real crystal (see Ref. 6, chapter 30), gives rise to considerable random multiple scattering in photonic crystals. A convenient way to study the transport of light in a multiple scattering system is enhanced backscattering.[61–63] The intensity scattered by an object exhibits a clear maximum in the exact backscatter direction, which results from constructive interference of counterpropagating light paths. It is well established that a triangular peak superimposed on the diffuse background results.[61–63] The width of this 'enhanced backscattering cone' is inversely proportional to the transport mean free path $\ell$. The transport mean free path is the length scale over which the direction of propagation of light is randomized and thus it quantifies the effect of disorder in the medium on the propagation of light. The transport mean free path limits the useful size range of photonic crystals for applications. An alternative method to obtain the transport mean free path is to measure the total transmission (*i.e.*, diffuse and coherent intensity transmitted by the sample integrated over all forward angles). A set of data as a function of sample thickness is needed to obtain the transport mean free path.

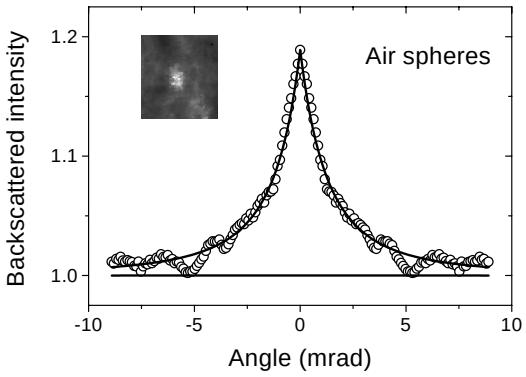


*Figure 10:* The backscattered intensity normalized to the diffuse background as a function of angle $\theta$ for an air-sphere crystal ($\lambda$ =460 nm) with a lattice parameter $360 \pm 10$ nm. The curve is a least-squares fit to the data of the cone shape predicted by diffusion theory for a disordered medium. For the air spheres we find the profile as a function of $|\theta|$ by integrating over circles concentric with the peak in the two-dimensional image (inset). The points $\theta < 0$ are duplicates of $\theta > 0$.[64]

We have measured enhanced backscattering from a $TiO_2$ air-sphere crystal for various wavelengths by collecting the backscattered intensity on a CCD camera positioned in the focal plane of a positive collection lens. A typical backscatter cone of an air-sphere crystal with lattice parameter $360 \pm 10$ nm is shown in Fig. 10.[64] The inset shows the two-dimensional image obtained from averaging multiple camera exposures. The backscatter cone shows as a bright spot compared to the diffuse background. The backscattered intensity as a function of $|\theta|$ is obtained by averaging over circles concentric with the intensity peak. To facilitate visual inspection, the data are plotted both for $\theta > 0$ and $\theta < 0$. The solid line is a least squares fit to the coneshape as predicted by diffusion theory.[63] From the width of the cone we typically obtain transport mean free paths of $15$ $\mu$m, which is equivalent to a distance of about 40 unit cells, or 70 lattice planes. Hence, the distance over which light becomes diffuse is so large that Bragg diffraction can easily build up. For opals of polystyrene spheres in air we find similar transport mean free paths.

The width of the cone is crucially influenced by the fact that the (111) planes are parallel to the sample surface in our experiment, resulting in L-gaps which coincide with the incident and backscatter direction. Starting from the diffusion equation for transport of light,[63, 65] we observe that the cone is affected by two different mechanisms, the first of which concerns the diffuse intensity. Light paths returning to the sample surface at directions close to normal incidence suffer from internal reflection due to Bragg diffraction. Internal reflection creates longer light paths, hence the cone becomes narrower.[65] The magnitude of the internal reflection effect is determined by the total solid angle of directions which are in a stop gap. This effect is maximal at the blue edge of the L-gap, and does not depend on the orientation of the sample with respect to the incident beam.

The second effect results from the attenuation of the coherent beam due to Bragg diffraction for frequencies in the L-gap. The cone is affected because the coherent beam acts as a source for the diffuse intensity. Due to the strong attenuation of the coherent beam at wavelengths within the stopband, the backscatter cone is predominantly composed of light paths starting very close to the sample surface. Since these light paths are shorter on average,[63] this effect broadens the cone. This effect only occurs if the incident and backscatter directions are chosen to match the Bragg condition, and depends strongly on the attenuation length, which we previously noted to be much longer than predicted by, e.g., a two-band model.

We have measured enhanced backscattering as a function of frequency[64] for opals and

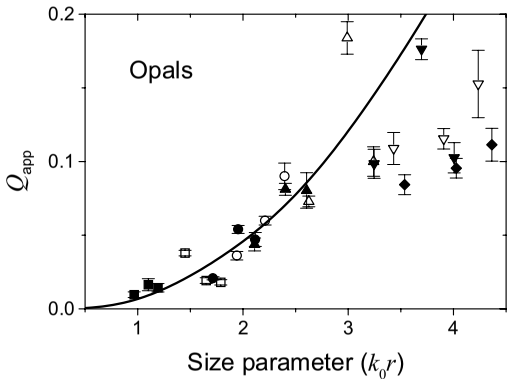


*Figure 11:* The apparent scattering efficiency per sphere $Q_{\rm app}$ as a function of the size parameter, for polystyrene opals made of particles with radii 120 (black squares), 180 (open squares), 213 (circles), 241 (open circles), 262 (black triangles), 326 (open triangles), 403 (downward black triangles), 426 (downward open triangles), 439 nm (black lozenges). The solid line is the Rayleigh-Gans scattering efficiency of a thin shell of refractive index 1 in an effective medium of refractive index 1.45.[64]

air-sphere crystals with the incident beam normal to the (111) planes. For frequencies below the L-gap, the cone width is not affected by either mechanism, since Bragg diffraction does not occur along any direction. For frequencies in the L-gap both mechanisms are relevant. Quantitatively the internal reflection effect dominates, leading to a net narrowing of the backscatter cone. For frequencies beyond the blue edge of the L-gap, the coherent beam is not Bragg diffracted, while the fraction of oblique propagation directions decreases continuously. The cone width, which is minimal at the blue edge of the L-gap, increases for increasing frequency. One may measure the attenuation effect, and hence the attenuation length, by choosing a frequency beyond the blue edge of the L-gap and recording backscatter cones as a function of incident and backscatter direction. The cone width will increase for the limited angular interval in which the incident direction matches the Bragg condition.

We have acquired enhanced backscattering cones for many opals of polystyrene spheres of different sizes for several wavelengths. Figure 11 (*cf.* Ref. 64) shows the apparent scattering efficiency $Q_{\rm app} = 1/(n\ell\pi r^2)$ of the spheres in the opals as a function of size parameter $2\pi r/\lambda$, where $r$ is the sphere radius, $\lambda$ the wavelength, and $n$ the number density of spheres in the opals. The apparent scattering efficiency increases with increasing sizeparameter.[32] As a simple model we propose that the scattering in the opals is mainly due to polydispersity of the spheres and small displacements from their lattice sites. The difference in refractive index profile of the displaced, slightly polydisperse Mie-spheres as compared to the ideal structure is a collection of thin shells of air and polystyrene. We have calculated the scattering efficiency[66] of spherical shells of refractive index 1 and radius $r$ in a homogeneous medium with the effective index of refraction of the opals (1.45). As shown in figure 11, this simple shell model compares well to the data for shell thicknesses which are $5\ \%$ of the nearest neighbor distance between spheres in the crystal. This value is consistent with the small sphere polydispersity of $\sim 2\ \%$, and with the estimated root mean square displacement $u_{\rm RMS} \leq 3.5\%$.

From the discussion above we conclude that extinction of the coherent beam and the build-up of a diffuse intensity are intrinsic to photonic crystals. Especially for self-organized systems, the size randomness of the building blocks sets the length scale over which light becomes diffuse, irrespective of the degree of ordering, to be at most 40 unit cells.

Disorder in photonic crystals has an important effect on the emission spectra of internal sources.[28] We have identified that disorder considerably reduces the attenuation for internal

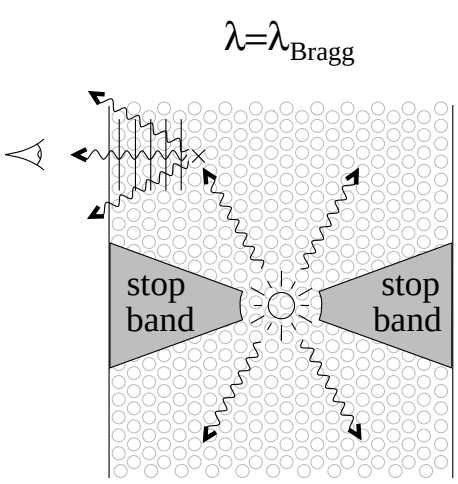


*Figure 12:* Schematic drawing of the trajectory of light emitted by a point source inside a photonic crystal if the light is just Bragg diffracted by the crystal planes indicated. The cross indicates a defect close to the surface of the crystal.[28]

sources in the frequency range of a stop gap (cf. Figs. 4, 6, and 7). The relevant mechanism is depicted in Fig. 12: light emitted in the direction of a stop gap is attenuated, but the light can propagate perfectly well in other directions. The light will be scattered by a small concentration of defects that always occur in any crystal. If light is scattered by defects close to the surface of the crystal, this radiation will appear unattenuated outside, even in the direction of a stopgap, because the light traverses only a thin layer of photonic crystal. Thus, light appears in the direction of a stop gap and the attenuation appears reduced.

## 6 ABSORPTION

Absorption is highly detrimental for photonic band gap effects. One of the main goals with photonic band gap crystals is to control excitations of atoms or molecules at time scales at least comparable with the excited state lifetime $\tau$. If the atoms have radiative lifetimes $\tau \sim$ nsec typical of dipole oscillators with $100\%$ quantum efficiency, then in a time $\tau$ light propagates for $\sim 10^6$ periods, or over a distance of $\sim 10^6$ wavelengths. Hence, the absorption length $l_{\rm abs}$ should be large: $l_{\rm abs} > 10^6\lambda$. For rare-earth atoms, with $\tau \sim$ msec, the requirement is even more stringent by another 6 orders of magnitude. Whether one can observe a Bragg diffraction from a crystal (see for instance Zakhidov *et al.*'s beautiful shiny graphite crystals[17]) is not a very rigorous measure for absorption, because a Bragg diffraction can build up within of the order of 10 layers pathlength, i.e., 10 wavelengths (back and forth). Thus, an absorption length $l_{\rm abs} > 10\lambda$ reveals Bragg diffraction, but will allow only a tiny effect on lifetimes.

The effect of enhanced backscattering is very sensitive to any effect that cuts off long light paths, because the top of the cone consists of contributions from very high scattering orders ($> 10^3$ scattering events, ı.e., light paths of at least $10^3\ell$, of order $\sim$cm). Both finite sample thickness and absorption result in a rounding of the backscatter cone,[67, 60] which is cusped for infinite non-absorbing media. We have recorded enhanced backscattering from polystyrene opals (see Fig. 13, Ref. 64) using the off-centered rotation technique,[68] which allows a high angular resolution of 0.3 mrad. Disregarding this finite resolution, the rounding of the cone top, shown in the inset of Fig. 13, allows us to conclude that the diffuse absorption length $L_a$ is more than 500 $\mu$m, which exceeds the sample thickness of 300 $\mu$m. The diffuse absorption length measures the average distance between starting and ending points of a

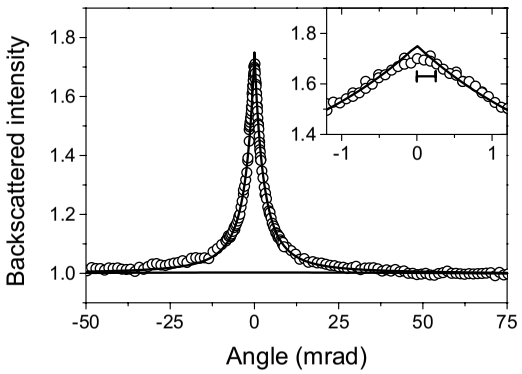


*Figure 13:* The backscattered intensity normalized to the diffuse background as a function of angle $\theta$ for an opal composed of polystyrene spheres of radius 180 nm measured at a wavelength of 685 nm. The curve is a least-squares fit to the data of the cone shape predicted by diffusion theory for a disordered medium. The inset shows a close up of the top. The horizontal bar indicates the high angular resolution.[64]

random light path over which the intensity decays by a factor $1/e$ as a result of absorption. Hence, the absorption length $l_{\rm abs}$, *i.e.*, the average length of such a path, is at least longer than 0.5 cm. Since the rounding in the inset of Fig. 13 is clearly comparable to the finite resolution of the setup, we conclude that the value quoted above underestimates the absorption length by at least an order of magnitude. The important conclusion is that the random multiple scattering is a useful probe to show that the absorption length indeed exceeds the relevant wavelengths by six orders of magnitude in polystyrene opals.

## 7 STRONG INTERACTION

The previous sections have mostly dealt with weakly photonic crystals, for which the edge frequencies of a stop gap increase with angles of incidence away from the normal, following the well-known Bragg law. With increasing crystal photonic strength and increasing frequency, light can diffract from more than one set of lattice planes simultaneously and entirely new physics is revealed. Here we illustrate two profound ways in which Bragg's law breaks down for strongly photonic crystals. First, we find from reflectivity data taken as a function of angle from the normal to the (111) face that although the lowest frequency gap (associated with the L-stopgap) obeys Bragg's law for small angles, for angles starting near $35^\circ$ a single reflectivity peak splits into two peaks indicating coupling of Bragg reflection processes from *two* planes, *viz.*, (111) and (200) crystal planes.[39] Second, at much higher frequencies in the vicinity of the region for which $2^{\rm nd}$ order Bragg reflection from (111) planes might occur, we observe three reflectivity peaks which do not change significantly with angle. We argue that multiple Bragg diffraction from *large numbers* of lattice planes results in band repulsions between Bloch states causing the frequencies of the edges of the stop gaps to become independent of angle of incidence.[40] One of the peaks is the precursor of a full photonic band-gap that would occur in a material of even higher dielectric contrast ($> 7.8$) than the titania air spheres. Multiple Bragg diffraction and low-dispersion Bloch modes have recently also been observed in emission spectra of light sources inside photonic crystals.[54]

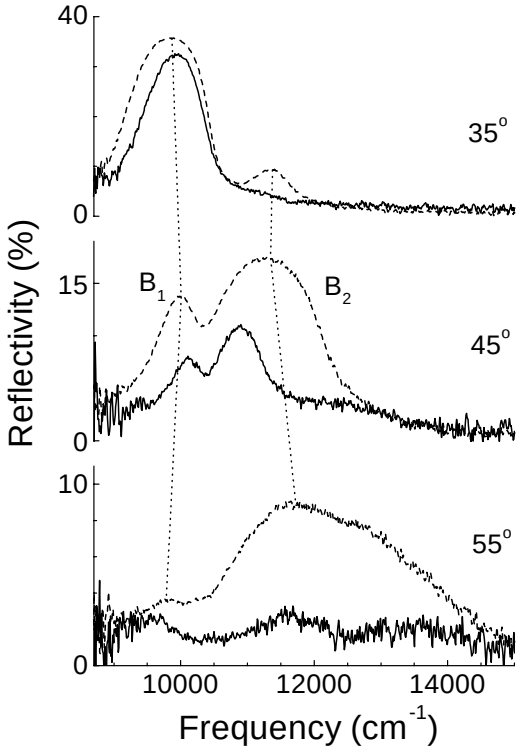


*Figure 14:* Bragg-reflection spectra for light incident on a crystal with $a = 860$ nm at angles of 35°, 45° and 55° for s- (dashed curves) and p-polarization (solid curves). The curves are offset, as shown by the left-hand scales. The vertical dotted lines are guides to the eye for the s-polarized peaks. $B_1$ and $B_2$ label the main peaks in both s- and p-polarized spectra.[39]

### 7.1 Coupling of Several Bragg Reflections

In the experiments designed to probe the spectral dependence of the reflectivity as a function of beam incidence angle ($\alpha$), we find that for both s- and p-polarization a single peak associated with the L-stop-gap occurs at 8700 cm$^{-1}$ for $\alpha$ =0°. This peak which we label as $B_1$ shifts to about 10000 cm$^{-1}$ at $\alpha$ =30°, in agreement with simple Bragg diffraction. For angles between 35° and 55° a much more complex behavior is observed as shown in Fig. 14. The $B_1$ peak becomes narrower and weaker between $\alpha$ =35° and 55°, and even decreases in frequency at higher $\alpha$. Starting at $\alpha$ =30°, a new peak, called $B_2$, appears at 11400 cm$^{-1}$. It first shifts down and then up in frequency, while becoming stronger and broader. There is also evidence for a weaker peak but we shall not concentrate on them here. The different polarizations show striking differences: for s-polarization, $B_2$ appears at a lower angle, and at $\alpha$ =45° this peak has a 400 cm$^{-1}$ higher frequency, a larger width and a higher amplitude compared to p-polarization. Beyond 55°, a single broad peak occurs in the s-polarized spectra while the p-polarized peaks have disappeared. The overall decrease of the p-spectra amplitudes relative to those of the s-spectra is probably due to the air-crystal boundary conditions for the electric and magnetic fields. The fact that the peaks do not reach ideal (100 %) reflectivity is probably related to a mosaic spread as well as diffuse scattering.

Figure 15 shows the center frequencies of all peaks as a function of $\alpha$ and demonstrates that the frequencies of $B_1$ and $B_2$ display an avoided crossing centered near 10500 cm$^{-1}$. The figure also shows the full widths at half maximum of the reflection peaks, that gauge the widths of stop gaps in the dispersion relations. The large frequency separations between the peaks in the avoided crossing region is similar to the widths of the peaks, a characteristic of

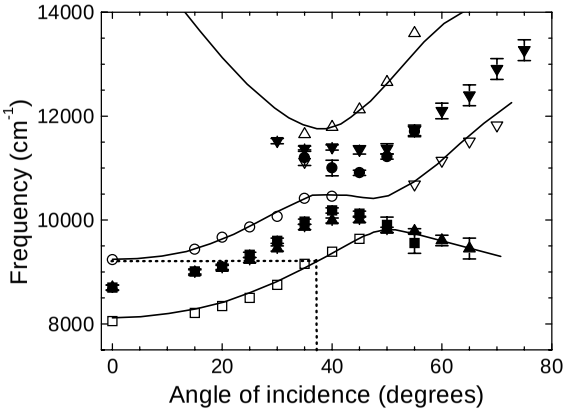


*Figure 15:* Frequencies of Bragg peaks as a function of angle of incidence for a crystal with $a = 860$ nm. Center frequencies are indicated by closed symbols: triangles for $B_1$-s polarized, squares are for $B_1$-p, inverted triangles are for $B_2$-s, and circles for $B_2$-p. The estimated error bars of the peak centers are indicated. Open symbols are half heights for the s-polarized $B_1$ peaks (squares and circles) and for the $B_1$ peaks (inverted and normal triangles). The drawn curves are calculated Bloch modes (s-polarized), converted to angle of incidence by parallel wave vector projection.[39] The dashed lines indicate the frequencies at top of the L-gap (at $0°$), that are Bragg diffracted all the way up to $37°$.[18]

coupled wave phenomena. We attribute the avoided crossing behavior to coupling of Bragg reflection events from (111) and (200) planes. This coupling also flattens the photon dispersion relations. Figure 16 shows the surface of the first Brillouin zone of the *fcc* structure, the surface associated with Bragg diffraction. For simple diffraction from real space (111) planes, the incident ($\mathbf{k}_{in}$) and reflected wave vectors ($\mathbf{k}_r$) lie on parallel (111)-type faces of the zone surface, with $\mathbf{k}_r = \mathbf{k}_{in} + \mathbf{G}$, with $\mathbf{G}$ the $hkl = 111$ reciprocal lattice vector. The angle *inside* the crystal is equal to the angle between $\mathbf{k}_r$ and $\Gamma$-L, or to the angle between $\mathbf{k}_{in}$ and a vector from $\Gamma$ to L. Diffraction occurs on the surface of the 1st Brillouin zone for small angles, and moves into the 2nd zone as $\mathbf{k}_{in}$ moves beyond the U point with increasing $\alpha$. If $\mathbf{k}_{in}$ passes through the U point (for intermediate $\alpha$), two diffracted wave vectors appear simultaneously: $\mathbf{k}_r$ on the (111) Bragg plane and $\mathbf{k}'_r$ on the (200) plane. In multiple Bragg diffraction, the diffracted waves are coupled, hence both diffraction processes are modified compared to simple Bragg diffraction. The occurrence of two or more coupled Bragg diffraction processes accounts for our experimental observations.

We have calculated the photonic dispersion curves by solving the Maxwell equations using the well-known plane wave expansion technique. The dielectric function for the crystal is represented by $\varepsilon(\mathbf{r}) = \sum \epsilon_{\mathbf{G}} \exp(\mathrm{i}\mathbf{G} \cdot \mathbf{r})$, where the sum extends over all reciprocal lattice vectors $\mathbf{G}$. Each of the eigenmodes for frequency $\omega$ and wave vector $\mathbf{k}$ is represented as $E^{\omega}_{\mathbf{k}}(r,t) = \exp(-\mathrm{i}\omega t) \sum E^{\omega}_{\mathbf{k},\mathbf{G}} \exp[\mathrm{i}(\mathbf{k} - \mathbf{G}) \cdot \mathbf{r}]$. Using a variety of analytical models for $\varepsilon(\mathbf{r})$, we find that the dispersion relations of the low-frequency modes relevant to us can be computed with *only three* distinct $\epsilon_G$, *viz.*, $\epsilon_0$, $\epsilon_{(111)}$, and $\epsilon_{(200)}$ (along with their symmetry related equivalents). We take $\epsilon_0 = 1.41$ from the square of the effective refractive index of 1.18. The 1200 cm$^{-1}$ width of the Bragg peak at $\alpha = 0°$ fixes $\epsilon_{(111)} = -0.18$. We have chosen $\epsilon_{(200)} = 0.1\epsilon_{(111)}$, guided by a model of close-packed air spheres, although variations of this coefficient by 50 % shift the dispersion curves less than 5 %. The calculated band-structures are converted to an external angle of incidence by parallel wave vector considerations and plotted in Fig. 15. At low angles and low frequencies, the two bands are mainly mixed (000) and (111) bands that bound the (111) Bragg diffraction. The band at high frequencies and low angles is a (200) mode. With increasing angle, the bands move together and obtain mixed character. Beyond 55°, the bands have changed character: the lowest mode is now the (200)

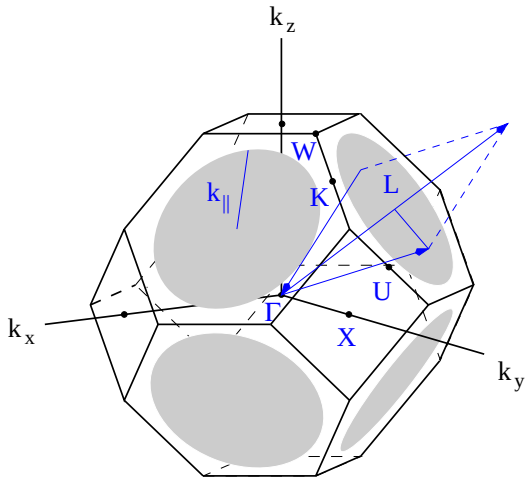


*Figure 16:* The first Brillouin zone of the *fcc* structure of the air-sphere crystals. Γ indicates the origin of reciprocal space, and K, L, U, and W are high symmetry points on the edge of the Brillouin zone. The arrow from the zone edge to Γ denotes the wave vector of an incident light beam, and the arrow from Γ to the zone edge indicates the wave vector of a reflected light beam. The long arrow from Γ through L is the 111 reciprocal lattice vector that is probed in the experiment. The shaded circles with radius $k_{\|} = k_{\mathrm{L}} \times 0.59$ indicate the range of wave vectors for which light with a frequency at the top of the L-stop band is reflected.[18]

mode, whereas the upper two have become the mixed (000) and (111) bands. It is remarkable that the positions of the bands, that delimit the edges of stop bands, are in excellent agreement with the half heights of the reflectivity peaks. This supports the proposition from section 3.1 that FWHM are good measures of widths of stop bands, but now extended to non-zero angles of incidence.

In the present experiments, multiple Bragg diffraction is observed with a coupling band width of about 10 $\%$ and an angular range of more than 10°. For comparison, in delicate x-ray diffraction experiments on atomic crystals the characteric intensity modulations occur over an angular range of arc seconds. This difference is easily understood, since photonic interactions are 3 to 6 orders of magnitude stronger in the optical regime than in the x-ray regime. The strong interactions cause strong band repulsions and flat dispersion bands that are the basis to the formation of photonic band gaps in the optical regime. Conversely, an x-ray photonic band gap is unlikely to occur on account of the weak interactions. Of course there are other differences between optical and x-ray scattering. The former is based on macroscopic Maxwell equations and as our data above illustrate, polarization characteristics play a major role. X-ray scattering is based on the microscopic Maxwell equations, hence polarization effects are subtle.

On the Brillouin zone surface illustrated in Fig. 16, the shaded area is the region of $k$-space over which light at a frequency (8700 cm$^{-1}$) corresponding to the top of the L gap at $\alpha = 0°$ is reflected. The extent of this range can be estimated from the data in Fig. 15 which shows that the top of the reflectivity gap at $\alpha = 0°$ coincides with the bottom of the reflectivity gap near $\alpha = 37°$. Taking into account all eight (111) faces of the Brillouin zone, one finds that $2.2\pi$ solid angle of wave vectors are diffracted, i.e., light propagation is inhibited for more than $55$ $\%$ of all possible directions. It has been proposed that this strongly inhibited light propagation, observed earlier for crystals with a = 480 nm,[18] leads to large changes in the optical density of states, and hence to grossly altered emission characteristics.

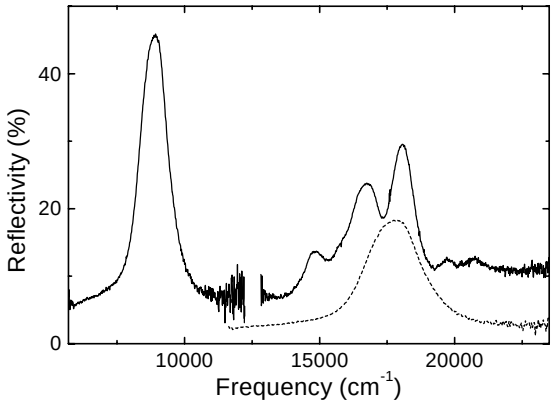


*Figure 17:* Reflection spectra for titania air-sphere crystals ($a = 860$ nm) at normal incidence as a function of frequency (solid curves). The peak at 8700 cm$^{-1}$ is the *fcc* (111) first order Bragg reflection. The three peaks at 14830, 16760, and 18070 cm$^{-1}$ are in the range of 2$^{\rm nd}$ order diffraction. For comparison, the dashed peak at 17600 cm$^{-1}$ is the (111) peak plotted at double the frequency (and reduced in reflectivity) as an estimate of a (222) 2$^{\rm nd}$ order Bragg peak in the weak photonic limit.[40]

### 7.2 Coupling of Multiple Bragg Reflections: Onset of a Complete Band-gap.

At higher frequencies than those associated with the L-stop gap, one can expect that Bragg coupling in a strongly photonic crystal will become much more complex, involving scattering from many planes and the formation of Bloch states with a multitude of plane wave components. The dispersion relations for certain Bloch modes can be expected to become flat over a large volume of k-space. For a crystal with an appropriate dielectric contrast ($>$7.8), it has been predicted that a complete photonic gap can occur.[21, 69, 70] One may wonder what experimental features are characteristic of a photonic band gap or even the onset of such.

In the titania air-sphere crystals, optical reflectivity measurements at normal incidence (Fig. 17) reveal three Bragg peaks at frequencies of 14800, 16700 and 18100 cm$^{-1}$, beyond the (111) 1$^{\rm st}$ order Bragg diffraction at 8700 cm$^{-1}$. It can be excluded that the triple peaks are due to disorder effects.[40] The new stop gaps occur in the frequency region where 2$^{\rm nd}$ order (222) Bragg diffraction would occur in a weakly photonic crystal, and where a complete photonic band gap is expected in a strongly photonic crystal. For comparison, in Fig. 17, we also plot the (111) 1$^{\rm st}$ order peak at twice its frequency to simulate a (222) 2$^{\rm nd}$ order peak. Clearly there is a marked difference in the weak and strong reflectivity signatures. In a weakly photonic crystal the peak reflectivity frequency would also be expected to obey Bragg's law. Figure 18 displays the high frequency component of the spectra at 0°, 15°, 30°, and 45°. Compared to normal incidence, the peaks in the 15° spectrum have broadened and shifted down by $\sim$500 cm$^{-1}$, the reflectivity is reduced, and a new component has appeared at 19200 cm$^{-1}$. At 30°, the overall spectrum has shifted to the blue, in qualitative agreement with Bragg behavior. The 14800 cm$^{-1}$ and the 16000 cm$^{-1}$ bands have disappeared, and there is a broad band centered at 17800 cm$^{-1}$. At 45°, there are bands at 18000, 19800, and 21000 cm$^{-1}$. The decrease in reflectivity amplitude with angle may be due to surface boundary conditions or multiple Bragg diffraction and grating modes that take light into non-specular directions.[71] The main observation, however, is that in strongly photonic crystals, the usual higher-order Bragg diffraction has changed to a complex coupling of many Bloch waves, that causes reflection bands to display little dispersion.

To obtain insight into our observations, we have computed the photonic band structures for our air-sphere crystals by the plane-wave expansion method for vector waves. We have used a spatially-dependent dielectric function $\varepsilon(\mathbf{r})$ that corresponds closely to the de-

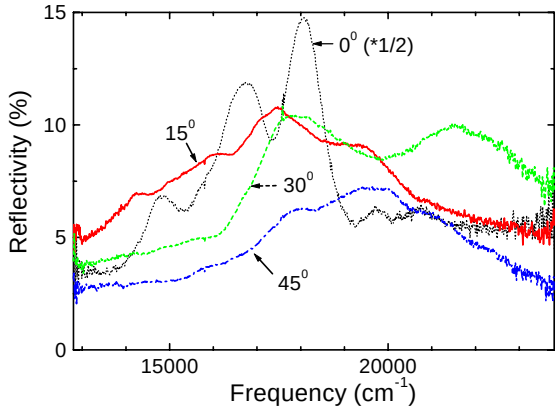


*Figure 18:* Reflection spectra of titania air-sphere crystals for angles of incidence of 0° (dotted curve, same as in Fig. 17 but multiplied by 0.5), 15° (solid curve), 30° (dashed curve), and 45° (dash-dotted curve).[40]

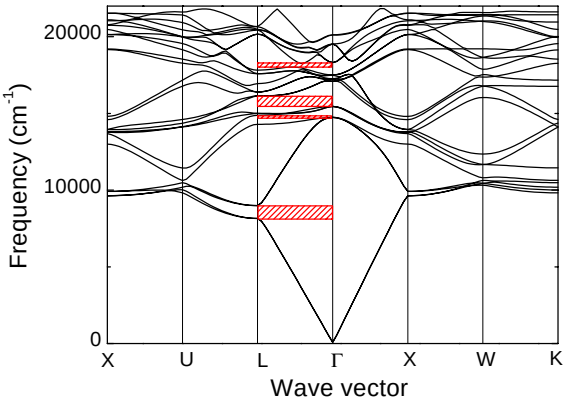


*Figure 19:* Photonic band structures for our titania air-sphere crystals ($a = 860$ nm), between common high-symmetry points in the Brillouin zone.[6] The results are computed with a model of dielectric shells with inner radius 1.0, outer radius 1.09, and connecting windows between the air spheres with radius 0.4. The dielectric constant of the $TiO_2$ is $\varepsilon = 6.5$, the lattice parameter is 860 nm, and 339 plane waves have been used. Stop gaps in the $\Gamma - L$ direction are indicated by hatched boxes.[40]

tailed structure obtained from SAXS and scanning electron microscopy experiments. The *fcc* crystals are well described by overlapping shells of dielectric material (titania), with inner radius 1.0 (touching close-packed air spheres) and outer radius 1.09 in units of the radius of close-packed spheres. This leaves the characteristic octagonal air voids seen, e.g., in SEM photographs. The air spheres inside the shells are connected to their twelve nearest neighbors by cylindrical windows with radius 0.4. The resulting $TiO_2$ filling fraction is $\varphi = 0.10$, the average for the samples considered. The dielectric constant of titania is taken as $\varepsilon = 6.5$, the isotropically averaged value for visible light. Bandstructures were calculated using up to 339 plane waves, although for the first 20 bands discussed here the frequencies are defined to better than 1% for as few as 120 plane waves.

Figure 19 shows the bandstructure for our crystals along high symmetry directions in the *fcc* Brillouin zone, calculated for $a = 860$ nm. We find three high frequency stop gaps beyond the $1^{st}$ order stop gap (8700 $cm^{-1}$) between the $\Gamma$ and L-points. These gaps can be directly compared to the reflectivity peaks at normal incidence, even though the peaks are somewhat asymmetrical: the gap between the 5th and the 6th bands centered at 14800 $cm^{-1}$

coincides well with the reflection peak at 14830 $cm^{-1}$, the gap between the 8th and the 9th bands centered at 15800 $cm^{-1}$ coincides reasonably with the reflectivity peak at 16760 $cm^{-1}$, and the gap between the 16th and 17th bands centered at 18100 $cm^{-1}$ coincides very well with the reflection peak at 18070 $cm^{-1}$. The results confirm theoretically that the observed phenomena are caused by many strongly coupled Bloch modes, associated with multiple Bragg diffraction.

Additional computations indicate how sensitive the high frequency gaps are to details of the topology of the model, *i.e.*, the details of $\varepsilon(\mathbf{r})$. If we eliminate the connecting windows altogether, while increasing the outer radius of the titania shells to $\sim 1.1$ to keep $\varphi$ constant, no high frequency stop-gaps occur. If we increase $\varphi$ to its maximum value (0.26) in a close-packed *fcc* crystal of air spheres and increase $\varepsilon$ of the backbone to 7.84, all three gaps survive but only the one between the 8th and 9th bands develops into a complete photonic gap, in agreement with earlier work.[21, 69] These results indicate that the reflectivity peak at 16700 $cm^{-1}$ is the precursor of the photonic band gap.

Calculations of the band structure along directions at an angle $\theta$ with respect to the $\Gamma - L$ direction, toward the U-point, indicate that the lowest stop-gap collapses for $\theta \sim 10^\circ$ while the two higher gaps collapse for $\theta \sim 15^\circ$. Although the theoretical gaps collapse in the same angular sequence and range as the experimentally observed decrease of the reflectivity peaks at 14830, 16760, and 18070 $cm^{-1}$, a quantitative comparison with experiment is a challenge. Since plane wave band structure calculations assume infinitely large crystals, effects caused by coupling of the light from outside to inside a crystal are neglected. Experimentally, wave vector projection effects are well understood in the range of first order diffraction, but these effects are compounded at higher frequencies, e.g., by grating modes (see below). This makes it difficult to directly compare external ($\alpha$) and internal ($\theta$) angles of propagation. Interpretation of the complex reflection patterns at high frequencies where the photonic band gap is expected, call for real-space calculations, such as finite difference time domain or transfer matrix techniques.

If momentum conservation parallel to the crystal surface is assumed in the frequency range of the newly observed peaks, the next Brillouin zone is reached at angles of about 30°. Hence the observed bands would be dispersionless over the whole face of the relevant Brillouin zone, a characteristic that might be expected for a crystal possessing a complete band gap. On the other hand, the band structures in Fig. 19 do not reveal a photonic band gap for the *fcc* titania crystals. These facts taken together warrant a note of caution in using reflectivity (or transmission) data to define a complete gap.

## 8 PROBES OF A PHOTONIC BAND GAP

At this point, the question arises what is suitable probe of a photonic band gap. One may consider cw reflectivity or transmission, to obtain stop gaps that overlap for all directions. While this method has been applied to the structures used in the microwave range,[8, 44] such a probe encounters challenges in the case of the promising air-sphere crystals, as we have seen in the previous section. Also, the high frequency bands relevant to fcc crystals may be "uncoupled" modes,[72, 73] and thus give rise to apparent stop gaps.

The first experimental probe of photonic band gaps proposed here is the study of the emission spectrum of light sources inside a photonic crystal.[28] We have seen above that in absence of a band gap, the attenuation in the transfer function is limited by scattering off defects near the samples' surface. This channel will be shut off in case of a photonic band gap, see Fig. 20, hence it is predicted that the transfer function will experience a complete attenuation in the frequency range of the gap.

The second band gap probe proposed here is to measure the radiative dynamics of light

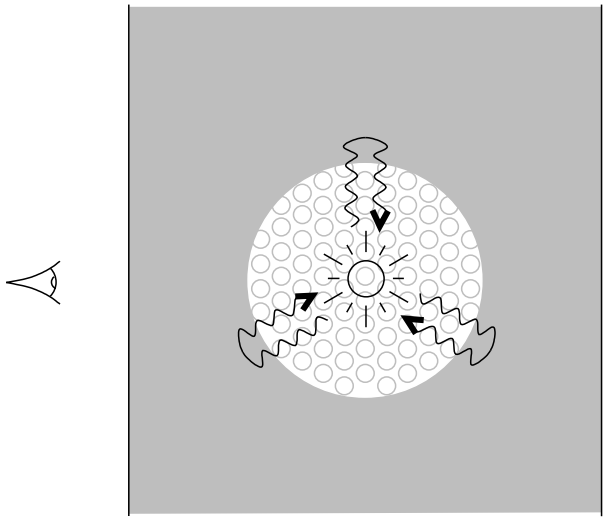

*Figure 20:* Schematic drawing of the trajectory of light emitted by a point source inside a photonic crystal with a photonic band gap. Locally the light can be emitted around a defect, but the light cannot propagate through the crystal. As a result, for the frequency range of the band gap, a notch is expected in the emission spectrum with a complete attenuation.[28]

sources inside photonic crystals.[3] This allows a direct access to the local density of states,[74] that will reveal a photonic band gap.[75]

Finally, a third probe is the measurement of the group velocity dispersion for all directions of propagation.[41] The gvd is an unambiguous probe of stop gaps, as it diverges at the edges of such gaps, and is very small inside of them. Thus, extensive gvd measurements allow the mapping of stop gaps for all directions, and hence, in case of overlap, a band gap.

## 9 ACKNOWLEDGMENTS

We are grateful to Judith Wijnhoven, Lydia Bechger, and earlier on Carlos van Kats for expert sample preparation, to Ad Lagendijk for continuous encouragements and support, to Henry Schriemer, Frank Schuurmans, Gijs van Soest, Rudolf Sprik, Michiel Thijssen, Gerard Wegdam for experimental help, discussions, and a great atmosphere, and to Theyencheri Narayanan, Peter Bösecke, and Olivier Diat for help at the ESRF. This work is part of research program of the “Stichting voor Fundamenteel Onderzoek der Materie (FOM)”, which is supported by the “Nederlanse Organisatie voor Wetenschappelijk Onderzoek” (NWO).

## REFERENCES

1. C.M. Soukoulis, ed., *Photonic Band Gap Materials*, Kluwer, Dordrecht (1996).

2. J.D. Joannopoulos, R.D. Meade, and J.N. Winn, *Photonic Crystals*, Princeton University Press, Princeton NJ (1995).

3. E. Yablonovitch, “Inhibited spontaneous emission in solid-state physics and electronics,” *Phys. Rev. Lett.* **58**, 2059 (1987).

4. S. John, “Strong localization of photons in certain disordered dielectric superlattices,” *Phys. Rev. Lett.* **58**, 2486 (1987).

5. R.W. James, *The Optical Principles of the Diffraction of X-rays*, Bell, London (1962).

6. N.W. Ashcroft and N.D. Mermin, *Solid State Physics*, Holt, Rinehart, and Winston, New York (1976).

7. W.L. Vos, R. Sprik, A. van Blaaderen, A. Imhof, A. Lagendijk, and G.H. Wegdam, “Strong effects of photonic band structures on the diffraction of colloidal crystals,” *Phys. Rev. B* **53**, 16231 (1996); erratum: *Ibid.* **55**, 1903 (1997).

8. E. Yablonovitch, T.J. Gmitter, and K.M. Leung, “Photonic band structure: the face centered cubic case employing nonspherical atoms,” *Phys. Rev. Lett.* **67**, 2295 (1991).

9. U. Grüning, V. Lehmann, S. Ottow, and K. Busch, “Macroporous silicon with a complete two-dimensional photonic band gap centered at 5 $\mu$m,” *Appl. Phys. Lett.***68**, 747 (1996).

10. T.F. Krauss, R.M. DeLaRue, and S. Brand, “Two-dimensional photonic bandgap structures operating at near-infrared wavelengths,” *Nature* **383**, 699 (1996).

11. S.Y. Lin, J.G. Fleming, D.L. Hetherington, B.K. Smith, R. Biswas, K.M. Ho, M.M. Sigalas, W. Zubrzycki, S.R. Kurtz, and J. Bur, “A three-dimensional photonic crystal operating at infrared wavelengths,” *Nature* **394**, 251 (1998).

12. N. Yamamoto, S. Noda, and A. Chutinan, “Development of one period of a three-dimensional photonic crystal in the 5-10 $\mu$m wavelength region by wafer fusion and laser beam diffraction pattern observation techniques,” *Jpn. J. Appl. Phys.* **37**, L1052 (1998).

13. A. Imhof and D.J. Pine, “Ordered macroporous materials by emulsion templating,” *Nature* **389**, 948 (1997).

14. O.D. Velev and E. Kaler, “Structured porous materials via colloidal crystal templating: from inorganic oxides to metals,” *Adv. Mater.* **12**, 531 (2000), and references therein.

15. B.T. Holland, C.F. Blanford, and A. Stein, “Synthesis of macroporous minerals with highly ordered three-dimensional arrays of spherical voids,” *Science* **281**, 538 (1998).

16. J.E.G.J. Wijnhoven and W.L. Vos, “Preparation of photonic crystals made of air spheres in titania,” *Science* **281**, 802 (1998).

17. A.A. Zakhidov, R.H. Baughman, Z. Iqbal, C. Cui, I. Khayrullin, S.O. Dantas, J. Marti, and V.G. Ralchenko, “Carbon structures with three-dimensional periodicity at optical wavelengths,” *Science* **282**, 897 (1998).

18. M.S. Thijssen, R. Sprik, J.E.G.J. Wijnhoven, M. Megens, T. Narayanan, A. Lagendijk, and W.L. Vos, “Inhibited light propagation and broad band reflection in photonic air-sphere crystals,” *Phys. Rev. Lett.* **83**, 2730 (1999).

19. A. Blanco, E. Chomski, S. Grabtchak, M. Ibisate, S. John, S.W. Leonard, C. Lopez, F. Meseguer, H. Miguez, J.P. Mondia, G.A. Ozin, O. Toader, and H.M. van Driel, “Large scale synthesis of a silicon photonic crystal with a complete three-dimensional photonic band gap near 1.5 micrometers,” *Nature* **405**, 437 (2000).

20. K. M. Ho, C. T. Chan, and C. M. Soukoulis, “Existence of a photonic gap in periodic dielectric structures,” *Phys. Rev. Lett.* **65**, 3152 (1990).

21. H.S. Sözüer, J.W. Haus, and R. Inguva, “Photonic bands: convergence problems with the plane-wave method,” *Phys. Rev. B* **45**, 13962 (1992).

22. M. Megens, C.M. van Kats, P. Bösecke, and W.L. Vos, “In-situ characterization of colloidal spheres by synchrotron small-angle x-ray scattering,” *Langmuir* **13**, 6120 (1997).

23. M. Megens, C.M. van Kats, P. Bösecke, and W.L. Vos, “Synchrotron small angle x-ray scattering of colloids and photonic colloidal crystals,” *J. Appl. Cryst.* **13**, 637 (1997).

24. W.L. Vos, M. Megens, C.M. van Kats, and P. Bösecke, “X-ray diffraction of photonic colloidal single crystals,” *Langmuir* **13**, 6004 (1997).

25. M. Megens, J.E.G.J. Wijnhoven, A. Lagendijk, and W.L. Vos, “Fluorescence lifetimes and linewidths of dye in photonic crystals,” *Phys. Rev. A* **59**, 4727 (1999).

26. M. Megens, Ph.D. thesis, Universiteit van Amsterdam (October 1999), available as pdf from our website.

27. A. Imhof, M. Megens, J.J. Engelberts, D.T.N. de Lang, R. Sprik, and W.L. Vos, “Spectroscopy of Fluorescein (FITC) dyed colloidal silica spheres,” *J. Phys. Chem. B* **103**, 1408 (1999).

28. M. Megens, J.E.G.J. Wijnhoven, A. Lagendijk, and W.L. Vos, “Light sources inside photonic crystals,” *J. Opt. Soc. Am. B* **16**, 1403 (1999).

29. M. Megens, H.P. Schriemer, A. Lagendijk, and W.L. Vos, “Comment on: Spontaneous emission of organic molecules embedded in photonic crystal,” *Phys. Rev. Lett.* **83**, 5401 (1999).

30. J.E.G.J. Wijnhoven, L. Bechger, and W.L. Vos, to be published.

31. J.E.G.J. Wijnhoven, S.J.M. Zevenhuizen, M. Hendriks, D. Vanmaekelbergh, J.J. Kelly, and W.L. Vos, “Electrochemical assembly of ordered macropores in gold,” *Adv. Mater.* **12**, 888 (2000).

32. M. Megens and W.L. Vos, “Excursions of particles in a colloidal crystal,” *Phys. Rev. Lett.* (submitted,2000).

33. W.L. Vos, R. Sprik, A. Lagendijk, G.H. Wegdam, A. Imhof, and A. van Blaaderen, “Dispersive effects on light scattering of photonic colloidal crystals,” *1994 European Quantum Electronics Conference, Postdeadline digest*, IEEE/LEOS, Piscataway NJ, (1994), paper EPD6.

34. W.L. Vos, J.E.G.J. Wijnhoven, and M. Megens, “Experimental probe of gaps in photonic crystals,” *Conference on Lasers and Electro-Optics Europe*, IEEE/LEOS, Piscataway NJ, 1998), paper CFB6.

35. W.L. Vos, M. Megens, C.M. van Kats, and P. Bösecke, “Transmission and diffraction by photonic colloidal crystals,” *J. Phys.: Condens. Matter* **8**, 9503 (1996).

36. K.W.K. Shung and Y.C. Tsai, “Surface effects and band measurements in photonic crystals,” *Phys. Rev.B* **48**, 11265 (1993).

37. R.J. Spry and D.J. Kosan, “Theoretical analysis of the crystalline colloidal array filter,” *Appl. Spectrosc.* **40**, 782 (1986).

38. A. Moroz and C. Sommers, “Photonic band gaps of three-dimensional face-centered cubic lattices,” *J. Phys.: Condens. Matter* **11**, 997 (1999).

39. H.M. van Driel and W.L. Vos, “Multiple Bragg wave coupling in photonic band gap crystals,” *Phys. Rev. B* **62**, 9872 (2000).

40. W.L. Vos and H.M. van Driel, “Higher order Bragg diffraction by strongly photonic fcc crystals: onset of a photonic bandgap,” *Phys. Lett. A* **272**, 101 (2000).

41. A. Imhof, W.L. Vos, R. Sprik, and A. Lagendijk, “Large dispersive effects near the band edges of photonic crystals,” *Phys. Rev. Lett.* **83**, 2942 (1999).

42. J.F. Bertone, P. Jiang, K.S. Hwang, D.M. Mittleman, and V.L. Colvin, “Thickness dependence of the optical properties of ordered silica-air and air-polymer photonic crystals,” *Phys. Rev. Lett.* **83**, 300 (1999).

43. Yu.A. Vlasov, V.N. Astratov, O.Z. Karimov, and A.A. Kaplyanskii, “Existence of a photonic pseudogap for visible light in synthetic opal,” *Phys. Rev. B* **55**, 13357 (1997).

44. E. Özbay, “Micromachined photonic band gap crystals: from microwave to far-infrared,” in: C.M. Soukoulis, ed., *Photonic Band Gap Materials*, Kluwer, Dordrecht (1996), p. 41.

45. A.M. Steinberg, P.G. Kwiat, and R.Y. Chiao, “Measurement of the single-photon tunneling time,” *Phys. Rev. Lett.* **71**, 708 (1993).

46. C. Spielmann, R. Szipocs, A. Stingl, and F. Krausz, “ Tunneling of optical pulses through photonic band gaps,” *Phys. Rev. Lett.* **73**, 2308 (1994).

47. M. Scalora, R.J. Flynn, S.B. Reinhardt, R.L. Fork, M.J. Bloemer, M.D. Tocci, C.M. Bowden, H.S. Ledbetter, J.M. Bendickson, and R.P. Leavitt, “Ultrashort pulse propagation at the photonic band edge: large tunable group delay with minimal distortion and loss,” *Phys. Rev. E* **54**, R1078 (1996)

48. Yu.A. Vlasov, S. Petit, G. Klein, B. Hönerlage, and C. Hirlimann, “Femtosecond measurements of the time of flight of photons in a three-dimensional photonic crystal,” *Phys. Rev. E* **60**, 1030 (1999).

49. R.H.J. Kop and R. Sprik, “Phase sensitive interferometry with ultrashort optical pulses,” *Rev. Sci. Instrum.*, **66**, 5459 (1995).

50. E. Lidorikis, Q. Li, and C.M. Soukoulis, “Optical bistability in colloidal crystals,” *Phys. Rev.E* **55**, 3613 (1997).

51. R.H.J. Kop, P. de Vries, R. Sprik, and A. Lagendijk, “Kramers-Kronig relations for an interferometer,” *Opt. Commun.* **138**, 118 (1997).

52. D. J. Heinzen, J. J. Childs, J. E. Thomas, and M. S. Feld, “Enhanced and inhibited visible spontaneous emission by atoms in a confocal resonator,” *Phys. Rev. Lett.* **58**, 1320 (1987).

53. S. Haroche, “Cavity quantum electrodynamics,” in *Systèmes fondamentaux en optique quantique/Fundamental systems in quantum optics*, Eds. J. Dalibard, J.-M. Raimond, J. Zinn-Justin, North-Holland, Amsterdam (1992).

54. H.P. Schriemer, H.M. van Driel, A.F. Koenderink, and W.L. Vos, "Modified spontaneous emission spectra of laser dye in inverse opal photonic crystals," *Phys. Rev. A. Rapid Comm.* **63** (January 1, 2001).

55. F. DeMartini, G. Innocenti, G. R. Jacobovitz, and P. Mataloni, "Anomalous spontaneous emission time in a microscopic optical cavity," *Phys. Rev. Lett.* **59**, 2955 (1987).

56. J. Martorell and N. M. Lawandy, "Observation of inhibited spontaneous emission in a periodic dielectric structure," *Phys. Rev. Lett.* **65**, 1877 (1990).

57. E. P. Petrov, V. N. Bogomolov, I. I. Kalosha, and S V. Gaponenko, "Spontaneous emission of organic molecules embedded in a photonic crystal," *Phys. Rev. Lett.* **81**, 77 (1998); "Modification of the spontaneous emission of dye molecules in photonic crystals," *Acta Phys. Pol. A* **94**, 761 (1998).

58. P.W. Anderson, "Absence of diffusion in certain random lattices," *Phys. Rev.* **109**, 1492 (1958); S. John, "Electromagnetic absorption in a disordered medium near a photon mobility edge," *Phys. Rev. Lett.* **53**, 2169 (1984).

59. D.S. Wiersma, P. Bartolini, A. Lagendijk, and R. Righini, "Localization of light," *Nature* **390**, 671 (1997).

60. F.J.P. Schuurmans, M. Megens, D. Vanmaekelbergh, and A. Lagendijk, "Light scattering near the localization transition in macroporous GaP networks," *Phys. Rev. Lett.* **83**, 2183 (1999).

61. Y. Kuga and A. Ishimaru, "Retroreflectance from a dense distribution of spherical particles," *J. Opt. Soc. Am. A* **8**, 831 (1984), M. P. van Albada and A. Lagendijk, "Observation of weak localization of light in a random medium," *Phys. Rev. Lett.* **55**, 2692 (1985); P. E. Wolf and G. Maret, "Weak localization and coherent backscattering of photons in disordered media," *Phys. Rev. Lett.* **55**, 2696 (1985).

62. E. Akkermans, P. E. Wolf, and R. Maynard, "Coherent backscattering of light by disordered media: Analysis of the peak line shape," *Phys. Rev.Lett.* **56**, 1471 (1986).

63. M. B. van der Mark, M. P. van Albada, and A. Lagendijk, "Light scattering in strongly scattering media: Multiple scattering and weak localization," *Phys. Rev. B* **37**, 3575 (1988).

64. A.F. Koenderink, M. Megens, G. van Soest, W.L Vos, and A. Lagendijk, "Enhanced backscattering from photonic crystals," *Phys. Lett. A* **268**, 104 (2000).

65. A. Lagendijk, R. Vreeker, and P. de Vries, "Influence of internal reflection on diffusive transport in strongly scattering media," *Phys. Lett. A* **136**, 81 (1989).

66. H. C. van der Hulst, *Light Scattering by Small Particles*, Dover, New York (1981).

67. P. Sheng, *Introduction to Wave Scattering, Localization, and Mesoscopic Phenomena*, Academic, San Diego (1995).

68. D. S. Wiersma, M. P. van Albada, and A. Lagendijk, "An accurate technique to record the angular distribution of backscattered light," *Rev. Sci. Instrum.* **66**, 5473 (1995).

69. K. Busch and S. John, "Photonic band gap formation in certain self-organizing systems," *Phys. Rev. E* **58**, 3986 (1998).

70. R. Biswas, M.M. Sigalas, G. Subramania, C.M. Soukoulis, and K.M. Ho, “Photonic band gaps of porous solids,” *Phys. Rev. B* **61**, 4549 (2000).

71. D. Labilloy, H. Benisty, C. Weisbuch, T.F. Krauss, D. Cassagne, C. Jouanin, R. Houdre, U. Oesterle, and V. Bardinal, “Diffraction efficiency and guided light control by two dimensional photonic band gap lattices,” *IEEE J. Quant. Electr.* **35**, 1045 (1999).

72. W.M. Robertson, G. Arjavalingam, R.D. Meade, K.D. Brommer, A.M. Rappe, and J.D. Joannopoulos, “Measurement of photonic band structure in a two-dimensional periodic dielectric array,” *Phys. Rev. Lett.* **68**, 2023 (1992).

73. K. Sakoda, “Group-theoretical classification of eigenmodes in three-dimensional photonic lattices,” *Phys. Rev. B* **55**, 15345 (1997).

74. R. Sprik, B.A. van Tiggelen, and A. Lagendijk, “Optical emission in periodic dielectrics,” *Europhys. Lett.* **35**, 265 (1996).

75. T. Suzuki and P.K.L. Yu, “Emission power of an electric dipole in the photonic band structure of the fcc lattice,” *J. Opt. Soc. Am. B* **12**, 570 (1995).